INTERNATIONAL JOURNAL FOR NUMERICAL METHODS IN ENGINEERING
Int. J. Numer. Meth. Engng 2003; **57**:1413–1430 (DOI: 10.1002/nme.783)

An element removal and reintroduction strategy for the topology optimization of structures and compliant mechanisms

T. E. Bruns[1,*,†] and D. A. Tortorelli[1,2]

[1]*Department of Mechanical and Industrial Engineering, University of Illinois at Urbana-Champaign, Urbana, IL 61801, U.S.A.*
[2]*Department of Theoretical and Applied Mechanics, University of Illinois at Urbana-Champaign, Urbana, IL 61801, U.S.A.*

SUMMARY

A method is developed to systematically remove and reintroduce low density elements from and into the finite element mesh on which the structural topology optimization problem is defined. The material density field which defines the topology and the local 'stiffness' of the structure is optimally distributed via non-linear programming techniques. To prevent elements from having zero stiffness, an arbitrarily small lower bound on the material density is typically imposed to ensure that the global stiffness matrix does not become singular. While this approach works well for most minimum compliance problems, the presence of low density elements can cause computational problems, particularly in structures that exhibit geometric non-linearities, e.g. in compliant mechanisms. To resolve this problem, a systematic approach for removing and reintroducing low density elements is presented, and the substantial performance improvements both in design and computational efficiency of the method over current methods are discussed. Several structures and compliant mechanisms are designed to demonstrate the method.

KEY WORDS: low density element; topology optimization; structural design; compliant mechanisms

1. INTRODUCTION

The goal of the structural topology problem [1] is to determine the optimal distribution of material, i.e. the material density distribution η, within a design domain that minimizes a given cost function and satisfies a series of constraint functions. Here, the design domain is defined by a continuum discretized by finite elements. A density design variable d_i (component i of the design variable vector $\mathbf{d}$) ranging continuously from zero to one, i.e. from void to solid material, is assigned to each finite element i by the optimization algorithm. The problem is most naturally posed as an integer design variable problem, i.e. $d_i = 1$ for solid and $d_i = 0$ for void elements. Unfortunately, such discrete formulations are ill-posed as they

*Correspondence to: T. E. Bruns, Department of Mechanical and Industrial Engineering, University of Illinois at Urbana-Champaign, Urbana, Illinois 61801, U.S.A.
†E-mail: tbruns@acm6.me.uiuc.edu

do not lead to convergent solutions. There are several methods that can be used to remedy the ill-posedness [1]. Here, the design space is restricted by filtering the design variable distribution to obtain the material density field (refer to Bruns [2] for the methodology and convergence studies and to Bourdin [3] for the proof of the well-posedness of the method).[‡] Rather than solving an integer programming problem, we use continuously varying design variables so that computationally efficient non-linear programming methods, e.g. the method of moving asymptotes (MMA) [4], can be used to solve the optimization problem. However, to approximate the effects of the discrete problem, the material density is penalized so that intermediate material densities are less desirable.

In this regard, a material density measure η_i is assigned to every finite element i and is defined by applying a filter to the density design variable field $\mathbf{d}$, i.e.

$$\eta_i = \hat{\eta}_i(\mathbf{d}) \tag{1}$$

The material density distribution affects the element stiffness because the strain energy function $\tilde{e}$ is defined as the product

$$\tilde{e}(\mathbf{E}(\mathbf{X},\mathbf{d}),\mathbf{X},\mathbf{d}) = (\gamma + (1-\gamma)\hat{\eta}_i^p(\mathbf{d}))\hat{e}(\mathbf{E}(\mathbf{X},\mathbf{d}),\mathbf{X}) \tag{2}$$

where $\mathbf{E}$ is the Green–St. Venant strain tensor, $\mathbf{X}$ is the position vector, and p and γ are parameters described below. For example and without loss of generality, we use a St. Venant–Kirchhoff material model so that

$$\hat{e} = \frac{vE}{2(1+v)(1-2v)}\,\mathrm{tr}(\mathbf{E})^2 + \frac{E}{2(1+v)}\,\mathrm{tr}(\mathbf{E}^2) \tag{3}$$

where the Young's modulus E and Poisson's ratio v are material parameters. The penalty parameter $p \geqslant 1$ penalizes intermediate material densities and is incremented throughout the optimization via a continuation method. The lower energy bound $\gamma\hat{e}$, defined by the parameter γ, eliminates the singularities that would otherwise arise in the finite element analysis when regions of low density material, i.e. regions where $\eta \to 0$, appear as the optimization progresses.[§]

The small lower bound on the elastic energy poses no computational problems in the presence of low density elements for most topology optimization problems, i.e. structures which exhibit small deformation. However, excessive distortion occurs in regions with low density elements in finite deformation analyses. Therefore, as the topology develops, finite elements can collapse or invert, and their element tangent stiffness matrices lose their positive definiteness. Moreover. excessive nodal displacements lead to numerical convergence problems in the analysis. To combat this problem, several approaches have been investigated.

[‡] Although we are seeking solid and void designs, intermediate material densities invariably appear in our topologies. One approach is to interpret the density distribution as the probability of finding solid material in any specific location in the domain, and then a solid and void topology is generated by post-processing the results accordingto appropriate threshold levels. There are several other methods [5, 6] that generate more distinct solid-void regions at other costs.

[§] Alternatively, a small non-zero lower bound $\underline{d}_i$ is commonly imposed on the density design variables, i.e. $0 < \underline{d}_i \leqslant d_i$. However, the lower bound on the material density decreases at a disproportionate rate as the penalty parameter p increases throughout the optimization continuation procedure, and therefore, unless $\underline{d}_i$ is sufficiently large, convergence problems in the structural analysis may be encountered.

One means of avoiding the above mentioned problems is to impose stress or buckling constraints on the elements so that a sufficient load carrying capacity of each element is maintained. The stress in intermediate density elements, and low density elements in particular, undergoing large deformation should be penalized in comparison to solid elements in the same deformation so that the optimization algorithm can distribute material in and around these highly stressed regions or eliminate them all together. Unfortunately, this method proves to be difficult to implement because an appropriate measure of stress in low and intermediate density elements is not apparent. Refer to Reference [7] for a more thorough discussion of stress constraints in topology optimization.

Alternatively, the low density elements can be artificially strengthened by prescribing the elastic energy such that low density elements cannot deform unrealistically. For example, to obtain better behaviour in compression, the St. Venant–Kirchhoff material is modified as

$$\hat{e} = \frac{vE}{2(1+v)(1-2v)} \operatorname{tr}(\mathbf{E})^2 + \frac{E}{2(1+v)} \operatorname{tr}(\mathbf{E}^2) + \beta h \tag{4}$$

where h is a function of the ratio between the deformed and undeformed differential volumes, i.e. of the determinant of $\mathbf{F}$ where $\mathbf{F}$ is the deformation gradient, and $\beta \geqslant 0$ is a penalty-like parameter. We have used a function of the form $h(\det(\mathbf{F})) = (\det(\mathbf{F}))^{-1} + 0.5(\det(\mathbf{F}))^2 - 1.5$ [8]. Another approach we have implemented to combat the low density element distortion problem is to limit the deformation of these elements by constraining the angles between the deformed element edges. This approach requires an active set strategy to limit the large number of angle constraints in the optimization problem. Both of these methods perform well if the optimization algorithm redistributes the material density to sufficiently carry the load in these high distortion regions in subsequent iterations. Unfortunately, both of these approaches adversely affect the topology design for the sole purpose of solving the analysis.

Another approach is to relax the convergence criteria in the non-linear structural analysis. Nodal degrees of freedom surrounded by low density elements can experience excessive displacements which lead to convergence problems during the finite element analysis. Buhl *et al.* [9] report that their convergence problems are remedied by removing these degree of freedom components from the equilibrium residual vector before taking its norm and by these same degrees of freedom when taking the displacement update norm. However, since it is not clear how these neglected degrees of freedom affect the analysis, we simply relax the convergence criteria, i.e. the absolute convergence tolerances on the norms of the residual and displacement updates are relaxed by several orders of magnitude, after a prescribed number of equilibrium iterations, e.g. 15. Fortunately, all that is necessary are structural and sensitivity analysis solutions at intermediate stages of the optimization where this non-convergence problem manifests itself. These methods do not suffer the drawback of the previous methods. However, the disadvantage of these methods, as well as the previous methods, is that the low density elements still have a non-negligible effect on the load carrying capacity of the structure.

Our treatment of low density elements so far has been to design structures in which the low density elements are structurally insignificant to the extent that the structural analysis can be performed. In the case of compliance minimization, these elements can nonetheless carry non-negligible loads. In the case of compliant mechanisms which undergo finite deformations, the presence of low density elements can adversely hinder or help in the topology design. For example, they help by carrying the load in intermediate designs in those regions which

would otherwise collapse, but because of this, they restrict desired motion. Here, we introduce a method to remove low density elements altogether from the topology optimization.¶ In this way, we circumvent all the disadvantages of the previous methods, we gain computational efficiency, and we generate better designs. Since elements are removed from the finite element computations, the computational time is reduced. This is particularly advantageous for problems where the analysis comprises a large portion of the computational overhead of the topology optimization, e.g. for non-linear finite element analyses. In addition, the optimal topology is not dependent on the initial mesh on which the topology optimization problem is solved since extraneous regions are systematically removed. Further, the process of extracting the topology from the mesh in the post-processing phase is straightforward, and more importantly, since the low density elements are removed, the resultant topology designs are better.

In Section 2 we discuss the procedure for removing and reintroducing elements. The implementation of the method is described in Section 3. Several structural and compliant mechanism topology designs that are obtained by this method are presented in Section 4.

2. LOW DENSITY ELEMENT REMOVAL AND REINTRODUCTION METHOD

Two fundamental issues must be addressed in methods that remove low density elements from the finite element mesh on which the topology optimization problem is defined. Firstly, the method must allow previously removed elements to be reintroduced into the mesh as the topology optimization progresses. Secondly, the method must suppress rigid body deformation modes that will invariably develop due to the formation of structural islands as the topology optimization progresses.

In regard to the reintroduction, we take advantage of the filters that we use to regularize the topology optimization problem. The filter defines a material density distribution field η that smooths, i.e. blurs, the design density distribution. In our discrete problem, for each element i the filter kernel is defined as a function of the distance between its centroid position (x_i, y_i) and the surrounding element centroid positions (x_j, y_j).‖ Here, a mesh-independent Gaussian-weighted** filter is used, although other filters may be implemented, e.g. a linearly weighted kernel. The material density η_i for element i is given by

$$\hat{\eta}_i(\mathbf{d}) = \sum_j \frac{\omega_j(s_{ij})}{\omega_i} d_j \tag{5}$$

¶In a similar way albeit different approach to topology design, any element is rejected from or admitted into the mesh around existing elements based on some criteria, typically stress, in so-called 'hard-kill' or evolutionary structural optimization methods (see e.g. References [10–12]). However, while these approaches are intuitiveand yield practical results, they lack proof of optimality, and furthermore, the resulting structural designs may be highly nonoptimal [13].

‖Although a continuous filter can be defined and would undoubtedly perform better in terms of regularizing the topology optimization problem, for computational ease and efficiency we define discrete filters that are based on the element centroid positions.

**Mollifier functions based on the Gaussian kernel are frequently used to stabilize ill-posed problems [14].

$$\omega_j(s_{ij}) = \begin{cases} \dfrac{\exp(-(s_{ij}^2/2(\frac{r}{3})^2)}{2\pi(r/3)} & \text{for } s_{ij} \leqslant r \\ 0 & \text{for } s_{ij} > r \end{cases} \tag{6}$$

$$s_{ij} = ((x_j - x_i)^2 + (y_j - y_i)^2)^{\frac{1}{2}} \tag{7}$$

$$\omega_i = \sum_j \omega_j(s_{ij}) \tag{8}$$

Note that the design densities of only those elements for which $s_{ij} \leqslant r$ affect the material density of element i. Thus, the prescribed parameter r determines the region of smoothing. The key to our ability to remove and later reintroduce elements into the finite element mesh is to recognize from Equation (5) that η_i cannot be zero unless all the surrounding element densities d_j within the kernel are also zero. Consequently, if $\eta_i = 0$ because the optimization has equated the density design variables d_j of all of the elements j for which $s_{ij} \leqslant r$ to zero, then element i is removed from the structural analysis and sensitivity analysis. But, as the optimization progresses and the element density of one or more elements j with $s_{ij} \leqslant r$ exceeds zero, then $\eta_i > 0$, and the previously removed element i is reintroduced into the analysis. Nodal degrees of freedom for a node k are removed from the structural analysis when all elements which are defined by node k are eliminated.

In practice to speed the removal and reintroduction process, we remove or reintroduce elements based on the conditions that $\eta_i < \varepsilon_r$ or $\eta_i > \varepsilon_r$ respectively. The tolerance $\varepsilon_r > 0$ is a small number selected such that the subsequent discontinuous displacement sensitivities due to the nonzero ε_r (and the nonzero lower energy bound $\gamma\hat{e}$) do not adversely affect the gradient-based optimization iterations. If ε_r is too large, then the optimization algorithm may chatter between successive designs with large regions of low density elements removed and subsequently reintroduced during early optimization iterations. This effect is more pronounced in the topology optimization with non-linear analysis than with linear analysis and more noticeable in compliant mechanism design than in stiffest structural design. Although further examination of the effects of the ε_r selection is warranted, the optimal topology designs do not significantly vary with ε_r from our experience. Moreover, on the infrequent occasions when ε_r is selected too large, the strategy loses robustness in the early optimization iterations, and therefore, we reduce the ε_r value and restart the optimization. For our examples, ε_r ranged between 0.01 and 0.05.

The removal and reintroduction of an element can be delayed by tracking its removal history to prevent toggling between its removal and reintroduction. If $\eta_i \leqslant \varepsilon_r$, then the removal history counter q_i for element i is incremented, and when $\eta_i > \varepsilon_r$, q_i is decremented. Once the removal history counter q_i exceeds a threshold number of iterations $\bar{q}$, then the element is removed. Previously removed elements are reintroduced when their counter drops below the threshold $\bar{q}$, or alternatively, the reintroduction is delayed until $q_i < \underline{q}$ where $\underline{q} < \bar{q}$, i.e. hysteresis. In addition, since low density elements cause numerical difficulties in the nonlinear structural analyses, the removal history counter q_i for low density elements with gross distortion, i.e. inversion or folding, is incremented to speed the rate at which these elements are removed from the mesh in the following optimization iterations.

As low density elements are removed, the connectivity of the structure changes dramatically. Invariably, rigid body deformation modes develop as regions of retained elements become

disconnected from the ground. To prevent the formation of disconnected regions, a constraint on the smallest eigenvalues of the stiffness matrix, i.e. $\lambda(\mathbf{K}) \geqslant \underline{\lambda} > 0$, can be applied. Unfortunately, the eigenvalue computations are costly, and the appropriate selection of the lower bound $\underline{\lambda}$ is problem dependent. Moreover, the eigenvalue constraints do not directly impose restrictions on the low density elements that cause the disconnection, and therefore, rigid body deformation modes may still develop.

As mentioned previously, since no information about the connectivity of the structure is known by the optimization algorithm, a means of accommodating rigid body deformation modes in the analysis must be included. One approach is to use image processing techniques to identify the paths between the applied loads and the ground. Disconnected regions are then discarded from the structural analysis. The advantage of this approach is that the topology can be readily interpreted, however this approach is computationally expensive. Another approach is to adopt analysis methods that accommodate the rigid body modes, e.g. the singular value decomposition. Unfortunately, while these approaches are less computationally expensive than the image processing approach, they are computationally expensive nonetheless, and further, an interpretation of the topology is obscured by such a purely numerical treatment.

We adopt an approach to resolve the rigid body deformation modes that is both numerically efficient and readily interpreted. The stiffness matrix is decomposed by Gaussian elimination with row pivotting, so all of the diagonal elements of the decomposed stiffness matrix are nonzero provided that the stiffness matrix is positive definite. When rigid body deformation modes are present, the stiffness matrix $\mathbf{K}$ loses its definiteness, and zeroes appear on the diagonal of the decomposed stiffness matrix $\tilde{\mathbf{K}}$. By associating these zeroes with their corresponding nodal degrees of freedom, we determine the nodal degrees of freedom to constrain in order to prevent the rigid body deformation modes. After the matrix equations are appropriately modified, the system equation can be solved. In this way, the rigid body deformation modes are removed from the analysis. More importantly, since these typically unloaded regions of mostly low density material are constrained from motion, they do not contribute to the performance of the structure or compliant mechanism, so the optimization algorithm tends to eliminate these regions in subsequent iterations.

As seen in the next section, the strategy described above can result in an intermediate topology in which the applied load is disconnected from the ground. The optimization algorithm may take advantage of this situation. To prevent this possibility, rather than constraining these degrees of freedom to zero displacement, these degrees of freedom can be prescribed to be finite displacements (that maintain the rigid body deformation) that are unfavorable to the optimization problem. For the topology optimization examples discussed in Section 4, topologies in which the loads are disconnected from the ground do not occur at intermediate optimization iterations.

3. IMPLEMENTATION

We now describe in more detail the implementation of the method to remove and reintroduce low density elements from the topology optimization. Without loss of generality, we illustrate the implementation of the element removal and reintroduction method on the linear truss system depicted in Figure 1. A similar method is employed for nonlinear continuum structural analyses.

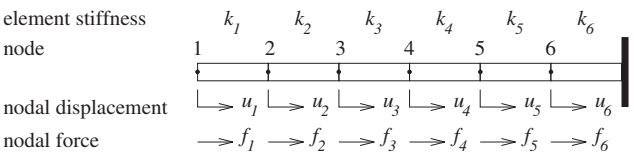

Figure 1. Six-node linear truss system.

Table I. Gaussian-weighted filter terms with radius $r = 1.5$.

Element j	1	2	3	4	5	6
s_{1j}	0	1	2	3	4	5
s_{2j}	1	0	1	2	3	4
s_{3j}	2	1	0	1	2	3
s_{4j}	3	2	1	0	1	2
s_{5j}	4	3	2	1	0	1
s_{6j}	5	4	3	2	1	0
$\omega_j(s_{1j})$	0.3183	0.0431	0	0	0	0
$\omega_j(s_{2j})$	0.0431	0.3183	0.0431	0	0	0
$\omega_j(s_{3j})$	0	0.0431	0.3181	0.0431	0	0
$\omega_j(s_{4j})$	0	0	0.0431	0.3181	0.0431	0
$\omega_j(s_{5j})$	0	0	0	0.0431	0.3181	0.0431
$\omega_j(s_{6j})$	0	0	0	0	0.0431	0.3183
ω_i	0.3614	0.4045	0.4045	0.4045	0.4045	0.3614

Following common notation, the governing system of equations for the truss system that behaves linearly, i.e. small elastic deformations, is

$$\mathbf{K}(\mathbf{d})\,\mathbf{U}(\mathbf{d}) = \mathbf{F} \tag{9}$$

where $\mathbf{K}$ is the global stiffness matrix, $\mathbf{U}$ is the nodal displacement vector, and $\mathbf{F}$ is the applied load vector. Each truss element i with linear stiffness k_i is weighted by a density measure $\hat{\eta}_i(\mathbf{d})$ where $0 \leqslant d_i \leqslant 1$ such that the element stiffness matrix is

$$\mathbf{K}^e = \eta_i^p \begin{bmatrix} k_i & -k_i \\ -k_i & k_i \end{bmatrix} \quad \text{with } k_i = \frac{A_i E_i}{L_i} \tag{10}$$

where A_i, E_i, and L_i are the element area, Young's modulus, and length, respectively, and $\gamma = 0$ in Equation (2). Here, each truss element has unit length, i.e. $L_i = 1$ for $i = 1, \ldots, 6$. The Gaussian-weighted filter coefficients of Equation (5) are given in Table I. The filter smooths the density design variables d_j of the $j = 1, \ldots, 6$ elements to define the element material density η_i for each element i. The filter radius $r = 1.5$ limits the smoothing neighbourhood of each element to its immediate neighbours.

Table II. Density measures η_i at optimization iteration m.

Element i	1	2	3	4	5	6
Design variable d_i	1	0	0	0	0	1
Density measure η_i	0.8808	0.1065	0	0	0.1065	0.8808

Following traditional finite element methodology, we (i) initialize the problem, (ii) assemble the global terms, i.e. **K** and **F**, and (iii) solve the resulting equation, i.e. Equation (9). As a component of the first step, we determine the nodal degree of freedom vector and the number of degrees of freedom. For our example, each node has one displacement degree of freedom. Therefore, the degree of freedom vector $\mathrm{DOF} = \{1,2,3,4,5,6\}^{\mathrm{T}}$, and there are six degrees of freedom, $\mathrm{NDOF} = 6$. In step (ii), we assemble the governing equation, cf. Equation (9), which for our example is

$$\begin{bmatrix} \eta_1^p k_1 & -\eta_1^p k_1 & & & & \\ -\eta_1^p k_1 & \eta_1^p k_1 + \eta_2^p k_2 & -\eta_2^p k_2 & & & \\ & -\eta_2^p k_2 & \eta_2^p k_2 + \eta_3^p k_3 & -\eta_3^p k_3 & & \\ & & -\eta_3^p k_3 & \eta_3^p k_3 + \eta_4^p k_4 & -\eta_4^p k_4 & \\ & & & -\eta_4^p k_4 & \eta_4^p k_4 + \eta_5^p k_5 & -\eta_5^p k_5 \\ & & & & -\eta_5^p k_5 & \eta_5^p k_5 + \eta_6^p k_6 \end{bmatrix} \begin{Bmatrix} u_1 \\ u_2 \\ u_3 \\ u_4 \\ u_5 \\ u_6 \end{Bmatrix} = \begin{Bmatrix} f_1 \\ f_2 \\ f_3 \\ f_4 \\ f_5 \\ f_6 \end{Bmatrix} \tag{11}$$

where $\mathbf{U} = \{u_1, u_2, u_3, u_4, u_5, u_6\}^{\mathrm{T}}$ and $\mathbf{F} = \{f_1, f_2, f_3, f_4, f_5, f_6\}^{\mathrm{T}}$. In the third step, the global stiffness matrix **K** is decomposed using Gaussian elimination, and the primal analysis is solved. Note that the decomposed **K** matrix is subsequently used in the design sensitivity analysis.

In order to remove void elements from the analysis, we modify the degree of freedom vector **DOF** and the number of degrees of freedom NDOF every optimization iteration. If the density measures for *every* element j connected to a node i admit

$$\eta_j \leqslant \varepsilon_r \tag{12}$$

then nodal degree of freedom i is removed from the degree of freedom vector **DOF**. For our example, the threshold value is set to $\varepsilon_r = 0$.

Here, the density design variables d_i and consequently the density measures η_i at optimization iteration m are given in Table II. Since node $i = 4$ is surrounded by element density measures that meet the criteria of Equation (12), the degree of freedom associated with node four is removed from degree of freedom vector, i.e. the fourth nodal degree of freedom is constrained to zero displacement as depicted in Figure 2, and we now have $\mathrm{DOF} = \{1,2,3,5,6\}^{\mathrm{T}}$

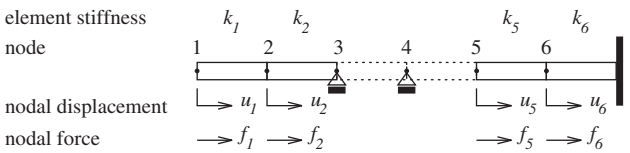

Figure 2. Removal of rigid body modes from linear truss system.

and NDOF = 5. The resultant $\mathbf{K}$ before and $\bar{\mathbf{K}}$ *after* Gaussian elimination are

$$\mathbf{K} = \begin{bmatrix} \eta_1^p k_1 & -\eta_1^p k_1 & & & \\ -\eta_1^p k_1 & \eta_1^p k_1 + \eta_2^p k_2 & -\eta_2^p k_2 & & \\ & -\eta_2^p k_2 & \eta_2^p k_2 & & \\ & & & \eta_5^p k_5 & -\eta_5^p k_5 \\ & & & -\eta_5^p k_5 & \eta_5^p k_5 + \eta_6^p k_6 \end{bmatrix} \tag{13}$$

and

$$\bar{\mathbf{K}} = \begin{bmatrix} \eta_1^p k_1 & -\eta_1^p k_1 & & & \\ 0 & \eta_2^p k_2 & -\eta_2^p k_2 & & \\ & 0 & 0 & & \\ & & & \eta_5^p k_5 & -\eta_5^p k_5 \\ & & & 0 & \eta_6^p k_6 \end{bmatrix} \tag{14}$$

In the course of decomposing $\mathbf{K}$ by Gaussian elimination with row pivoting, a zero diagonal element, i.e. zero within working precision, is encountered, hence there is a rigid body deformation present. Here, the third diagonal element of $\bar{\mathbf{K}}$ is zero, i.e. zero within working precision, and hence we remove the rigid body deformation mode by constraining the third nodal degree of freedom from the analysis as depicted in Figure 2. To remove rigid body deformation modes, we reassemble the governing system equation, and we impose constraints of zero displacement on the targeted degrees of freedom. For our example, the third row and column of the *reassembled* $\mathbf{K}$ and the third row of $\mathbf{F}$ are zeroed, and the respective diagonal element is equated to one, i.e. the resultant equation becomes

$$\begin{bmatrix} \eta_1^p k_1 & -\eta_1^p k_1 & 0 & & \\ -\eta_1^p k_1 & \eta_1^p k_1 + \eta_2^p k_2 & 0 & & \\ 0 & 0 & 1 & 0 & 0 \\ & & 0 & \eta_5^p k_5 & -\eta_5^p k_5 \\ & & 0 & -\eta_5^p k_5 & \eta_5^p k_5 + \eta_6^p k_6 \end{bmatrix} \begin{Bmatrix} u_1 \\ u_2 \\ u_3 \\ u_5 \\ u_6 \end{Bmatrix} = \begin{Bmatrix} f_1 \\ f_2 \\ 0 \\ f_5 \\ f_6 \end{Bmatrix} \tag{15}$$

Table III. Density measures η_i at optimization iteration $m+1$.

Element i	1	2	3	4	5	6
Design variable d_i	0.75	0.25	0	0	0.25	0.75
Density measure η_i	0.8927	0.1852	0.0107	0.0107	0.1852	0.8927

where we recall that the degree of freedom due to node four was previously removed. Note that in general we must account for the row pivotting in the Gaussian elimination and that a similar zeroing of the right-hand-side terms in the design sensitivity analyses, i.e. in the pseudo or adjoint load vectors, is also necessary.

Once the structural analysis is complete, the low density void elements remaining in the analysis are checked to determine if they experience gross distortion. Since low order Gaussian quadratures with low order element shape functions, e.g. four Gauss points per four-node quadrilateral element, are typically utilized in the computation, the negative determinant of the deformation gradient, i.e. $\det(\mathbf{F})<0$, is generally not a reliable indicator of element inversion. We employ a more direct method by calculating the cross-product between pairs of adjacent edges of the deformed low density elements. If any of these products change direction, the removal history counter q_i is incremented so that the element removal is hastened.

If in the next optimization iteration $m+1$ the optimization algorithm redistributes material such that elements that have been removed no longer meet the criteria of Equation (12), then these elements are reintroduced into the mesh. For our example, if the density design variables are redistributed by the optimization algorithm according to Table III, then no element density measure η_i meets the removal criteria. Therefore, element three is reintroduced back into the mesh, i.e. $\mathrm{DOF}=\{1,2,3,4,5,6\}^{\mathrm{T}}$ and $\mathrm{NDOF}=6$, and there will be no rigid body deformations.

4. EXAMPLES

In this section, we demonstrate the low density element removal and reintroduction method as we design several structures and compliant mechanisms. Firstly, the designs of a cantilever beam and a simply supported beam with and without the removal strategy are compared. Secondly, the resulting topologies of the cantilever beam with mesh refinement are studied, and the computational requirements of removing vs not removing low density elements are compared. Lastly, the topology designs of compliant mechanisms using non-linear elastic structural analyses are presented.

4.1. Structures

The usual objective in the design of a structure is to minimize the compliance, or maximize the stiffness, under prescribed loading conditions. In addition, an upper bound $\bar{v}$ constraint is placed on the effective volume $v=\hat{v}(\mathbf{d})=\int_{V_o}\hat{\eta}(\mathbf{d})\,\mathrm{d}v$ of the structure to limit resources. The density design variables are allowed to vary between solid material and void. The topology

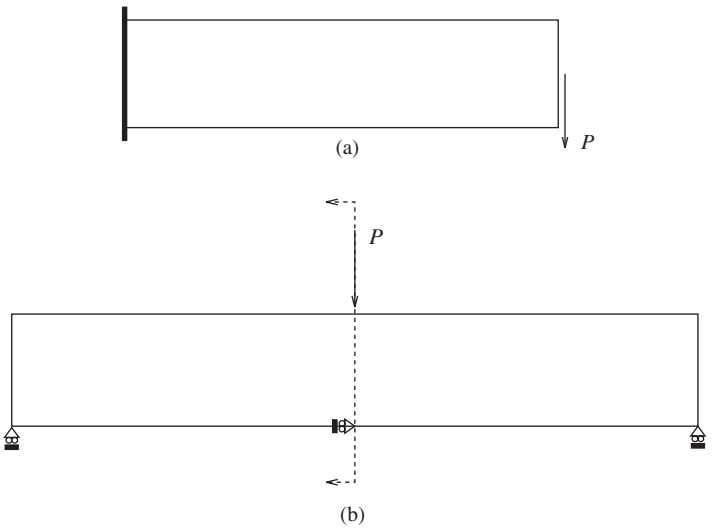

Figure 3. (a) Tip-loaded cantilever beam; and (b) midspan-loaded simply supported beam.

optimization problem, to be solved by the MMA, is stated as

$$\text{minimize} \quad \Theta_0(\mathbf{d}) \tag{16}$$

$$\text{subject to} \quad \Theta_i(\mathbf{d}) \leqslant 0 \tag{17}$$

$$\underline{d}_j \leqslant d_j \leqslant \bar{d}_j \tag{18}$$

where Θ_0 is the objective function, Θ_i (for $i = 1, \ldots$) are the inequality or equality constraints and d_j (for $j = 1, 2, \ldots$) are the design variables that are bounded above and below by $\bar{d}_j$ and $\underline{d}_j$.

A traversely tip-loaded cantilever beam with dead load $P = 10\,\text{N}$ is depicted in Figure 3(a). The $200\,\text{mm} \times 50\,\text{mm}$ domain (with 10 mm width) is discretized by a 80×20 4-node quadrilateral element mesh. Similarly, a simply-supported beam loaded at its midspan by dead load $P = 10\,\text{N}$ is depicted in Figure 3(b). The symmetric left half of the $600\,\text{mm} \times 50\,\text{mm}$ domain (with 10 mm width) is discretized by a 120×20 4-node quadrilateral element mesh. The material response is given by Equation (3) using the infinitesimal strain tensor and a Young's modulus $E = 2000\,\text{N/mm}^2$ and Poisson's ratio $v = 0.4$. The lower bound parameter $\gamma = 10^{-6}$ is set on the strain energy function e of Equation (2). Initially, the density design variables are equated to $d_j = 0.5$. The penalty parameter p is incremented in increments of 0.1 from 1.5 to 3.0 every 10 optimization iterations. The filter length r is set to 4.0 mm. With regard to Equations (16)–(18),

$$\Theta_0 = u_p \tag{19}$$

$$\Theta_1 = v - \bar{v} \tag{20}$$

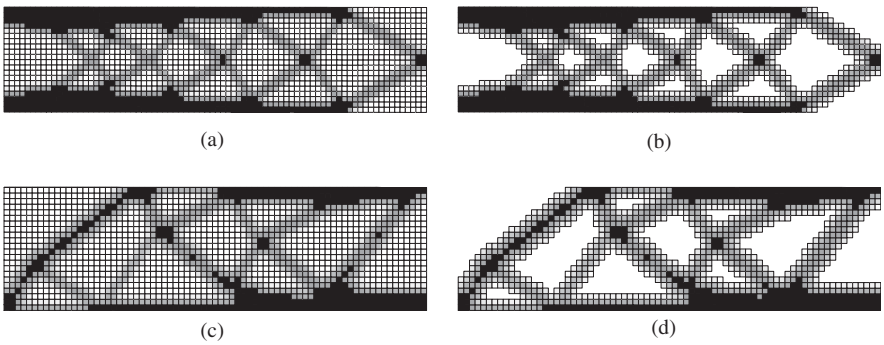

Figure 4. Topology plots of the density measures η of the tip-loaded cantilever beam: (a) without and (b) with element removal, and the midspan-loaded simply supported beam (c) without and (d) with void removal.

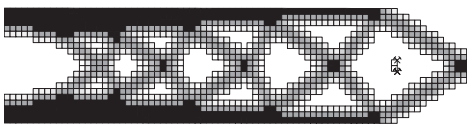

Figure 5. Constraining nodes to prevent rigid body motion.

$$\underline{d}_j = 0 \tag{21}$$

$$\bar{d}_j = 1 \tag{22}$$

where u_P is the component of the nodal displacement located at and in the direction of the applied dead load P. The upper bound on the effective volume $\bar{v}$ is set to 50% of the maximal volume, i.e. $\bar{v} = 0.50 v_{\max}$ where $v_{\max} = \int_{V_o} \mathrm{d}v$. For element removal and reintroduction, we use $\varepsilon_r = 0.05$ and $\bar{q} = \underline{q} = 0$.

The topologies that are based on linear analyses of the cantilever beam and simply supported beam are plotted in Figure 4. Figures 4(a), (c) and (b), (d) show the resultant topologies that are obtained with and without element removal. Note that the same topologies result and that the differences in the objective functions are indistinguishable, i.e. 0.2056 and 0.0534 mm for the cantilever beam and simply supported beam, respectively. However, the computational time is reduced by 16% (from an average of 1592–1331 cpu s) and 5% (from an average of 4824–4588 cpu s) for the cantilever beam and simply supported beam, respectively, using the element removal method on IBM RS/6000 SP thin nodes (133 MHz PPC 604 processors). In addition, the tedious task of extracting the topology in the post-processing stage is largely circumvented.

At iteration 174 of the topology optimization with the element removal method, rigid body deformation modes appear in the cantilever beam analysis. The removal of the rigid body motion is depicted in Figure 5 where the ⊗ symbol denotes that a nodal degree of freedom has been constrained to zero. Note that three degrees of freedom are fixed to prevent the translational and rotational motion of the two low density elements.

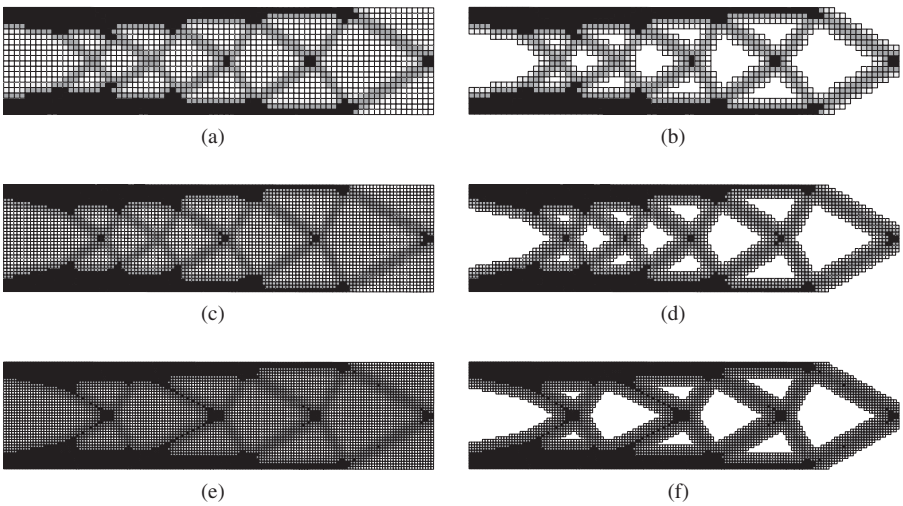

Figure 6. Topology plots of the density measures η of the tip-loaded cantilever beam (a), (c), (e) without and (b), (d), (f) with element removal for (a), (b) 80×20, (c), (d) 128×32, and (e), (f) 160×40 element meshes.

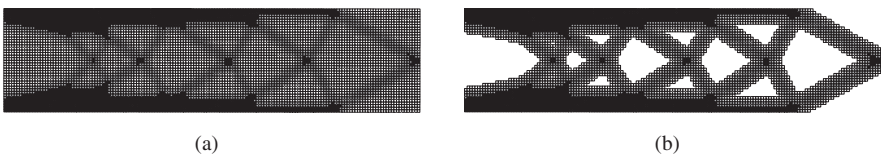

Figure 7. Topology plots of the density measures η of the tip-loaded cantilever beam (a) without and (b) with element removal with 160×40 element mesh. Here, there penalty parameter p is incremented after every 30 iterations rather than 10.

The resultant topologies for the mesh convergence studies of the tip-loaded cantilever beam appear in Figure 6. Again, note that the topologies obtained with and without element removal are comparable. In addition, the topologies are similar with mesh refinement. We attribute the convergence of the finest mesh discretization to a slightly different optimal topology to the continuation method. If the penalty parameter is increased after 30 rather than 10 iterations, then the resultant topology matches the topologies of the coarser meshes, cf. Figures 6 and 7. The computational efficiency with and without element removal for various mesh discretizations can be compared in Table IV.

4.2. Compliant mechanisms

Here, we design a gripper mechanism that undergoes large displacements, i.e. we use a nonlinear elastic analysis to accommodate the finite deformations (refer to Figure 8). The symmetric half of the 200 mm $\times$ 300 mm domain (with 10 mm width) is discretized by 4400 4-node quadrilateral elements. A linear spring is defined to simulate a workpiece with a stiffness of $k = 0.25\,\mathrm{N/mm}$. A 50 mm $\times$ 100 mm space accepts the workpiece to be gripped. The parameters for the material response and optimization are the same as those defined previously,

Table IV. Computational time vs mesh discretization.

Mesh discretization	Average time (cpu s)*		
	Without element removal	With element removal	(%) Reduction
80×20	1592	1331	16%
128×32	21039	19199	9%
160×40	89750	80893	10%

*IBM RS/6000 SP 133 MHz PPC 604 processor.

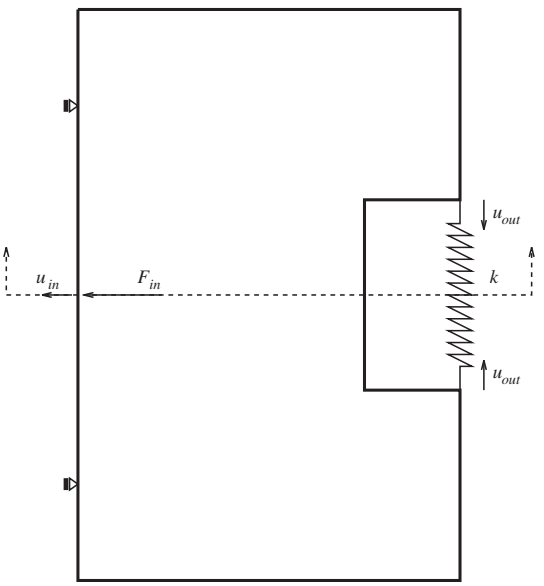

Figure 8. Gripper mechanism.

except the penalty parameter p is fixed at $p=3$ to hasten the optimization convergence. The objective is to synthesize the topology such that the gripper applies the largest gripping force F_{out}, and consequently largest output displacement u_{out}, on the workpiece with the least amount of input work $W_{\text{in}} = F_{\text{in}} u_{\text{in}}$ for a constant horizontal input force $F_{\text{in}} = 20\,\text{N}$. With regard to Equations (16)–(18),

$$\Theta_0 = u_{\text{in}} - u_{\text{out}} \tag{23}$$

$$\Theta_1 = v - \bar{v} \tag{24}$$

$$\underline{d}_j = 0 \tag{25}$$

$$\bar{d}_j = 1 \tag{26}$$

The upper bound on the effective volume $\bar{v}$ is set to 30% of the maximal volume, i.e. $\bar{v} = 0.30 v_{\max}$. The density design variables are fixed as solid material, i.e. $d_j = 1$, at the input

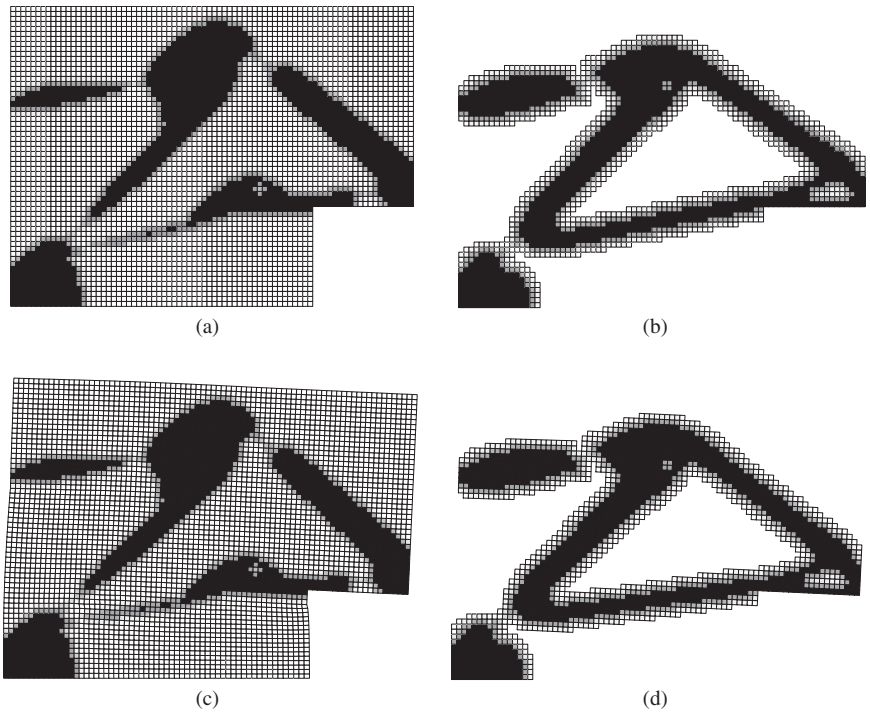

Figure 9. Topology plots of the density measures η of the symmetric half of the gripper mechanism (a), (c) without and (b), (d) with element removal in its (a), (b) undeformed and (c), (d) deformed configurations.

Table V. Comparison of optimal topology results of the gripper mechanism.

Topology optimization with non-linear elastic analyses	u_{in} (mm)	u_{out} (mm)	Optimization iterations*	Average time (cpu s)†
Without element removal	3.512	8.075	176	23501
With element removal	3.580	8.297	198	15847

*MMA
†IBM RS/6000 SP 133 MHz PPC 604 processor.

and output ports. Elements are removed from the computations if $\eta \leqslant \varepsilon_r = 0.01$. Note that ε_r is reduced because, as discussed previously, the optimization algorithm can be disrupted by the discontinuities in the gradient information, and this effect is more pronounced when using a non-linear analysis. All other parameters are equal to those used in the beam problems.

The symmetric halves of the resulting optimal topologies are shown in Figure 9 with and without element removal and in their undeformed and deformed configurations. Note that the structural members of the topology that is obtained with the element removal are thicker than those of the topology that is obtained without the element removal. We attribute this difference to the presence of low density elements which carry some load in the latter design. In Table V the results of the optimal topologies that are obtained with and without element removal are

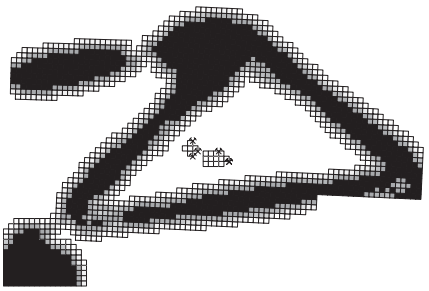

Figure 10. Constraining nodes to prevent rigid body motion.

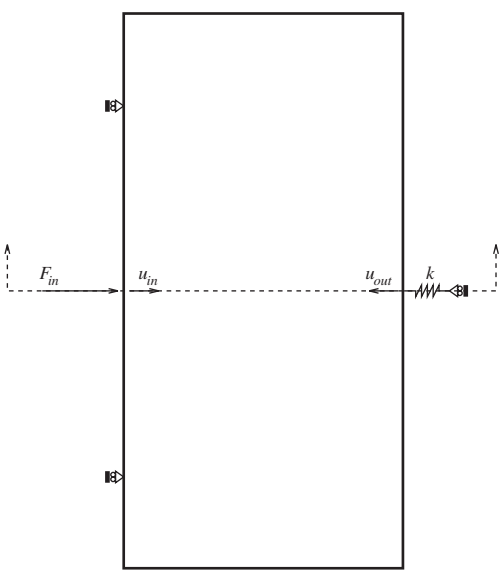

Figure 11. Inverter mechanism.

compared. Note that the computation time is reduced by 33% with the element removal method even though the number of optimization iterations actually increased by 12.5%. In the design of the compliant mechanisms, rigid body deformation modes appear frequently as the topology develops. For example, Figure 10 shows where the nodal degrees of freedom are constrained, denoted by the ⛌ symbol, in order to remove the rigid body motion of the gripper mechanism at optimization iteration 51.

Finally, we design an inverter mechanism that undergoes finite deformations using nonlinear elastic analysis (refer to Figure 11). The symmetric half of the 150 mm $\times$ 300 mm domain (with 10 mm width) is discretized by 3600 4-node quadrilateral elements. The linear spring that simulates the workpiece now has a stiffness of $k = 1\,\mathrm{N/mm}$. The objective is again maximize the mechanical efficiency of the mechanism, i.e. to displace the workpiece u_{out} as much as possible (in the opposite direction of the constant horizontal input force $F_{\mathrm{in}} = 20\,\mathrm{N}$) with the least amount of input work. The remainder of the problem definition is the same as the gripper mechanism example. The symmetric halves of the resulting optimal topologies that

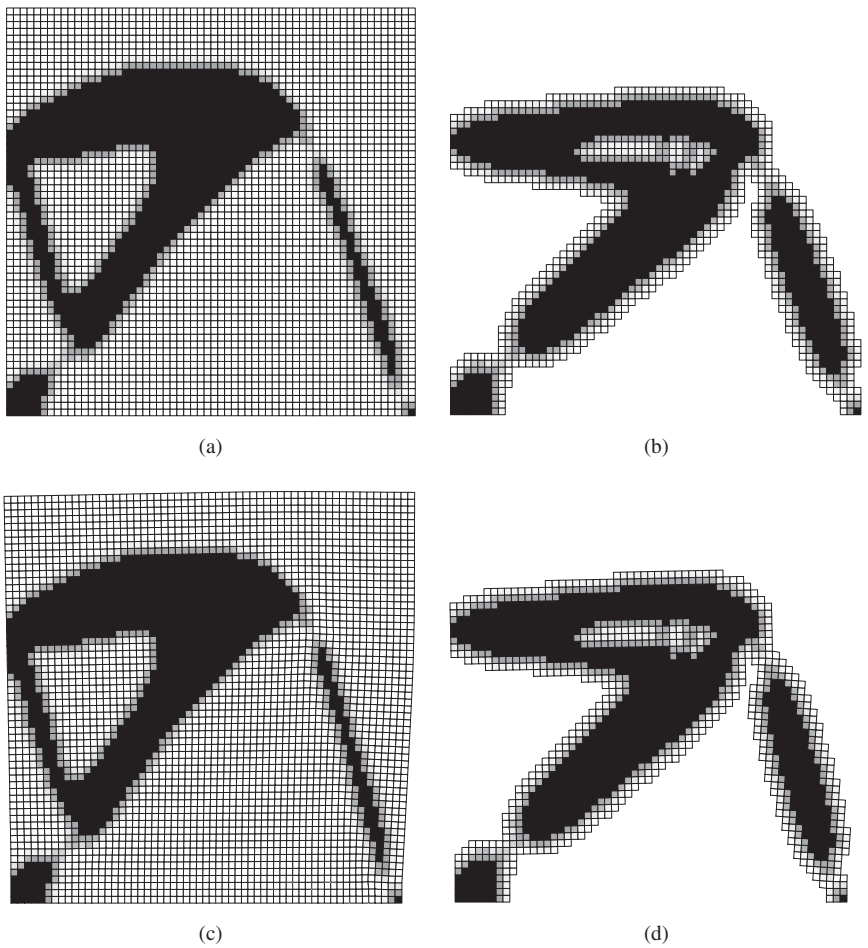

Figure 12. Topology plots of the density measures η of the symmetric half of inverter mechanism (a), (c) without and (b), (d) with element removal in its (a), (b) undeformed and (c), (d) deformed configurations.

are obtained with and without element removal appear in Figure 12 in their undeformed and deformed configurations. Again, note that the structural members of the topology that is obtained with element removal are thicker than the links of the topology that is obtained without the element removal. In Table VI the topology designs with and without element removal are compared. Here, the computation time is reduced by 78% with the element removal method.

5. CONCLUSION

A novel method to systematically remove and reintroduce low density elements in topology optimization is presented. The method offers several benefits. The tedious task of extracting the topology in the post-processing stage is largely circumvented, and the resultant topology

Table VI. Comparison of optimal topology results of the inverter mechanism.

Topology optimization with non-linear elastic analyses	u_{in} (mm)	u_{out} (mm)	Optimization iterations*	Average time (cpu s)†
Without element removal	1.575	4.915	658	71653
With element removal	1.677	5.086	266	15615

* MMA
† IBM RS/6000 SP 133 MHz PPC 604 processor.

reflects the true topology since structurally insignificant, albeit numerically significant, low density elements are removed from the structure. The computational time is reduced, particularly for designs that require non-linear elastic analyses. In addition, the initial design domain upon which the topology is developed can be arbitrarily defined since structurally useless regions are removed.

Because the ordering of the equations, i.e. **DOF** for Equation (9), to solve the structural analysis is based on the initial, arbitrary domain, further computational improvements will be examined by implementing optimal reordering equation procedures, e.g. Gibbs–Poole–Stockmeyer algorithm [15], to reduce the bandwidth. Furthermore, since relatively large motions of the formed links in the compliant mechanism are obtained, the method may need to consider contact. Finally, we note that the method can easily be extended to three dimensional problems, especially since the computational savings will make such computations tractable.

REFERENCES

1. Bendsøe MP. *Optimization of Structural Topology, Shape, and Material*. Springer-Verlag: New York, 1995.
2. Bruns TE, Tortorelli DA. Topology optimization of nonlinear elastic structures and compliant mechanisms. *Computer Methods in Applied Mechanics and Engineering* 2001; **190**(26–27):3443–3459.
3. Bourdin B. Filters in topology optimization. *International Journal for Numerical Methods in Engineering* 2001; **50**(9):2143–2158.
4. Svanberg K. Method of moving asymptotes—A new method for structural optimization. *International Journal for Numerical Methods in Engineering* 1987; **24**(2):359–373.
5. Sigmund O. On the design of compliant mechanisms using topology optimization. *Mechanics of Structures and Machines* 1997; **25**(4):493–524.
6. Borrvall T, Petersson J. Topology optimization using regularized intermediate density control. *Computer Methods in Applied Mechanics and Engineering* 2001; **190**(37–38):4911–4928.
7. Duysinx P, Bendsøe MP. Topology optimization of continuum structures with local stress constraints. *International Journal for Numerical Methods in Engineering* 1998; **43**(8):1453–1478.
8. Bruns TE, Tortorelli DA. Topology synthesis of geometrically nonlinear structures and compliant mechanisms. *Proceedings of the 7th AIAA/USAF/NASA/ISSMO Symposium on Multidisciplinary Analysis and Optimization* 1998; **AIAA-98-4950**:1874–1882.
9. Buhl T, Pedersen CBW, Sigmund O. Stiffness design of geometrically nonlinear structures using topology optimization. *Structural and Multidisciplinary Optimization* 2000; **19**(2):93–104.
10. Querin OM, Steven GP, Xie YM. Evolutionary structural optimisation (ESO) using a bidirectional algorithm. *Engineering Computations* 1998; **15**(8):1031–1048.
11. Reynolds D, McConnachie J, Bettess P, Christie WC, Bull JW. Reverse adaptivity—A new evolutionary tool for structural optimization. *International Journal for Numerical Methods in Engineering* 1999; **45**(5):529–552.
12. Liu JS, Parks GT, Clarkson PJ. Metamorphic development: a new topology optimization method for continuum structures. *Structural and Multidisciplinary Optimization* 2000; **20**(4):288–300.
13. Zhou M, Rozvany GIN. On the validity of ESO type methods in topology optimization. *Structural and Multidisciplinary Optimization* 2001; **21**(1):80–83.
14. Murio DA. *The Mollification Method and the Numerical Solution of Ill-posed Problems*. Wiley: New York, 1993.
15. Gibbs NE, Poole Jr WG, Stockmeyer PK. An algorithm for reducing the bandwidth and profile of a sparse matrix. *SIAM Journal on Numerical Analysis* 1976; **13**:236–250.

